Conformational Changes at the Tetramerization Site of Erythroid α-Spectrin upon Binding β-Spectrin: A Spin Label EPR Study†

Chloe Antoniou, Vinh Q. Lam,‡ and L. W.-M. Fung*

Department of Chemistry, University of Illinois at Chicago, 845 West Taylor Street, MC 111, Chicago, Illinois 60607

Received May 7, 2008; Revised Manuscript Received August 12, 2008

ABSTRACT: We used cysteine scanning, isothermal titration calorimetry (ITC) and spin label EPR methods to study the two regions that flank the partial domain Helix C′ of the N-terminal end of α-spectrin (residues 14−20 and residues 44−54) in the absence and presence of a model protein of the β-spectrin C-terminal end. In the absence of β-spectrin, residues 14−20 and 46−52 were known to be unstructured. The EPR spectral values of the inverse line width (ΔH^{-1}) and of the width between the low field peak and the central peak (*aZ*) of residues in part of the first unstructured region (residues 17−20) and of most residues in the second unstructured junction region (residues 46−52) changed dramatically upon association with β-spectrin, suggesting that the two regions undergo a conformational change, becoming more rigid and likely becoming helical. ITC results showed that three of the seven residues in the junction region (residues 46−52) were very important in its association with β-spectrin, in the following order: L49 > G46 > K48. In general, our results suggest that any mutations that affect the propensity of helical formation in the region spanning residues 17−52 in α-spectrin, or that affect hydrophobic clustering and/or salt-bridge stabilization of the bundled helices, would affect spectrin tetramer formation, and may lead to blood disorders.

Erythroid spectrin is a major component in the membrane skeleton of erythrocytes and plays a role in the major function of erythrocytes, as deformable and durable containers for hemoglobin and other molecules, by maintaining their unique biconcave shape. Two heterodimers of α- and β-spectrin associate to form a functional tetramer (*1*). The association involves a pair of identical interactions between the N-terminal region of the α-subunit and the C-terminal region of the β-subunit (*2, 3*). We have previously shown that a recombinant protein consisting of either the first 156 residues, including the partial domain and one structural domain, or the first 368 residues of α-spectrin, including the partial domain and three structural domains, may serve as a model protein to study the structure−function relationship of spectrin tetramerization, since both proteins associate with another recombinant protein consisting of residues 1898 to 2083 in the C-terminal region of β-spectrin (*3, 4*). Their association affinities are similar to those of intact α- and β-spectrin (*4*). The model protein consisting of 368 amino acid residues exhibits an unfolding behavior more similar to that of native α-spectrin than the one with 156 residues (*5*).

From sequence homology studies, it was predicted that the N-terminal region of α-spectrin consisted of a single helix (Helix C′, a partial structural domain) and was followed by a full triple helical domain (*6*). The prediction also suggested that two helices (Helix A′ and Helix B′, another partial domain) followed the last structural domain in β-spectrin. The bundling of the three helices (Helices A′, B′ and C′) is presumably responsible for two dimers associating to form a tetramer (*2, 7*). Our circular dichroism (CD[1]) data show that the unpaired helices that form the partial domains in the two model proteins of α- and β-spectrin become paired upon association (*3*), supporting the suggested mechanism of helical bundling of partial domain helices at the tetramerization region of αβ-spectrin. The CD data also show an increase in total helical content upon complex formation (*3*).

We have since determined the solution structure of this critical region, using the smaller model protein with the first 156 residues of α-spectrin (*8*). The structure consists of a single, well-defined helix formed by residues 21−45, which is preceded by a segment of 20 residues and followed by a segment of 7 residues that are unstructured. Thus, the NMR structure identifies Helix C′ as the helix spanning positions 21−45. The first structural domain is indeed a triple helical bundle, with the first helix (Helix A_1) starting at residue 53, and the last helix (Helix C_1) ending at residue 153. Since

† This work was supported, in part, by grants from the American Heart Association (0350617Z to L.W.-M.F.) and the National Institutes of Health (GM68621to L.W.-M.F.). The high resolution/high mass accuracy LTQ-FT mass spectrometer was supported by grants from the Searle Funds at the Chicago Community Trust to the Chicago Biomedical Consortium and the University of Illinois Chicago Research Resources Center.

* To whom correspondence should be addressed. E-mail: lfung@uic.edu. Tel: 1-312-355-5516. Fax: 1-312-996-0431.

‡ Current address: Division of Chemistry and Chemical Engineering, California Institute of Technology, Pasadena, CA 91125. Tel: 1-626-395-4071. Fax: 1-626-568-9430.

[1] Abbreviations: CD, circular dichroism; DTT, dithiothreitol; EPR, electron paramagnetic resonance; ITC, isothermal titration calorimetry; MTSSL, (1-oxy-2,2,5,5-tetramethyl-3-pyrrolinyl-3-methyl)methanethiosulfonate; R1, spin labeled cysteine residue; Spα, a recombinant protein consisting of residues 1−368 of erythroid α-spectrin; SpαΔ, single cysteine proteins derived from Spα; Spβ, a recombinant protein consisting of residues 1898−2083 of erythroid β-spectrin.

10.1021/bi800840p CCC: $40.75
Published on Web 09/11/2008

the residues following Helix C′ are in an unstructured conformation, the movement of Helix C′ is independent of the movement of the structural domain, a property that differs from published predictions that suggest Helix C′ to be connected to the first structural domain with a rigid helical segment (*9*). Our earlier spin label EPR studies of the first ten residues in Helix C′ suggest that residues with low side-chain mobility (on the hydrophobic face of Helix C′) are responsible for binding with β-spectrin (*10*). Our recent high resolution NMR studies of the smaller model protein of α-spectrin (156 residues) in an αβ-spectrin complex surprisingly reveal that residues outside Helix C′ are also involved in tetramerization (*11*). In the presence of β-spectrin, the motional properties of the residues in the unstructured regions flanking Helix C′ differ from those in the absence of β-spectrin. In this work, we spin labeled these residues as well as a few residues upstream and downstream of them, and used EPR methods to further understand the roles of these residues in spectrin tetramerization.

Our results indicate that the four residues (residues 17−20) prior to and seven residues (residues 46−52) after Helix C′ of erythroid α-spectrin undergo a conformational change from a highly flexible, unstructured to a more rigid conformation, possibly a helical conformation.

Mutations that disturb this helical bundling at the tetramerization site can lead to blood disorders such as hereditary elliptocytosis and pyropoikilocytosis. Many detrimental mutations lie within Helix C′ (residues 21−45) (*12*). However, mutations outside Helix C′ are also shown to be detrimental. For example, L49F has been shown to be a mutation producing clinical symptoms (*13, 14*). In a yeast two-hybrid system, we have shown that the L49H mutation abolishes interactions needed to form tetramers (*15*). Findings in this study provide a molecular mechanism for defective tetramer formation in patients with these mutations.

MATERIALS AND METHODS

DNA Constructs. The construct of the cysteine-less fragment of the first 368 residues of α-spectrin (*10, 16*) was used to prepare a family of single cysteine proteins, scanning residues 14−20 (14C−20C) and 44−54 (44C−54C). The DNA sequences of these proteins were verified by DNA sequencing analysis at the Research Resources Center (RRC) at the University of Illinois at Chicago (UIC).

Protein Preparation. The expression of all proteins as glutathione-*S*-transferase fusion proteins was induced by isopropyl β-D-1-thiogalactopyranoside. Only the expression of the cysteine residue at position 15 (replacing a native proline residue) was not achieved. Each fusion protein was cleaved by thrombin as reported previously (*17*). Thus, the native protein of α-spectrin with the first 368 residues (Spα) and its cysteine-less protein plus a total of 17 single cysteine proteins (SpαΔ), as well as a β-spectrin consisting of residues 1898−2083 (Spβ) (*11, 18*), were prepared. Protein concentrations were determined using absorbance values at 280 nm, with extinction coefficients determined from the primary sequence of each protein. The molecular mass of each protein was analyzed by high resolution mass spectroscopy (Washington University Resource for Biomedical and Bioinorganic Mass Spectroscopy, St. Louis, MO, and at RRC, UIC). CD spectra at 20 °C for all proteins were obtained using a JASCO 810 CD spectropolarimeter with a 0.1 cm path length. Mean residue molar ellipticity values at 222 nm were used to calculate the helical content of the proteins using a value of −36,000 deg cm^2 dmol^{-1} for a 100% helical conformation (*19*). The actual helicity values were probably higher, as we discussed recently in comparing the helicity values from CD and NMR studies (*11*).

Spin Labeling. Each SpαΔ, in 5 mM phosphate buffer with 150 mM NaCl (PBS), was incubated with dithiothreitol (DTT) at 37 °C for 1 h, followed by removal of DTT using gel filtration. A 3- to 5-fold molar excess of spin label (1-oxy-2,2,5,5-tetramethyl-3-pyrrolinyl-3-methyl)methanethiosulfonate (MTSSL) (Toronto Research Chemicals, Toronto, Canada) was added to the protein sample, and the mixture was stirred gently for 2−3 h at room temperature in the dark. Any excess of free MTSSL was removed by gel filtration. Each spin labeled protein was designated by its native amino acid residue, or its position in sequence and "R1", such as G14R1 or 14R1. The spin label concentration was determined by EPR, using a TEMPO calibration curve (Bruker user manual). To determine background labeling, a cysteine-less protein sample was processed in parallel. Generally ∼15% (0.15 label per molecule) background labeling was observed in cysteine-less samples. This amount of background spin label was subtracted from the raw spin label concentration, and the molar ratio of spin label to protein was calculated for each single cysteine protein sample. This background labeling seemed high, although it was similar to that in our earlier EPR studies of α-spectrin (*10*). About 5% of this signal was from glutathione trapped in the protein (*20*). About 10% signal remained after samples were treated with urea (6 M), followed by dialysis and column chromatography. The background signal remained similar in samples with and without β-spectrin.

Isothermal Titration Calorimetry. Isothermal titration calorimetry (ITC) measurements were performed at 25 °C using a VP ITC from MicroCal. All proteins were dialyzed in PBS and thoroughly degassed before each titration measurement. 14R1−20R1 and 44R1−54R1 (as titrants), ranging from 150 to 500 μM, depending on the affinity of each with Spβ, were titrated with Spβ (ranging from 20−30 μM; 1.4 mL). Injections of about 5−10 μL (depending on its affinity) for each titrant were made at 10 min intervals. The first injection point was usually not included in data analysis. The association equilibrium constant ($1/K_d$) was obtained from curve fitting using a single-site model provided by the ITC software.

Spin Labeled Samples. SpαΔR1 proteins in PBS with 40% glycerol (∼60 μM final protein concentration, with spin label to protein molar ratios ranging from 0.8 to 1), with and without Spβ, were used for EPR measurements. For the samples with Spβ, two molar excess Spβ was added to each sample except for 49R1, for which a five molar excess was added due to its low affinity with Spβ, as discussed below.

EPR Studies. EPR spectra of proteins were acquired with a 9.4 GHz Bruker EMX EPR spectrometer equipped with an HS4021 cavity at 20 °C, controlled by a variable temperature unit. Spin label signals in the raw EPR spectra from nonspecific, background labeling as discussed above were removed by computer subtraction. For the spectra with two molar excess of Spβ, the residual signals of the uncomplexed component (Spα alone), if present, were also

subtracted. The resulting spectra were then analyzed. The central line width (ΔH) and the width between the low field peak and the central peak (aZ, a value related to the value of the hyperfine separation, see Figure 3) of each spectrum of labeled protein alone and in the presence of the Spβ were measured. Usually, the hyperfine separation A_{zz} (the separation between the low field and high field peaks) parameter is measured. However, for the spectra of Spα in the complex, some of the high field signal(s) were not obvious. Thus, we used the separation between the low field peak and central peak, aZ, since it is a value related to the value of the hyperfine separation parameter and yet was easily quantified. The second moment of each spectrum ($\langle H^2 \rangle$) was also calculated directly from the first derivative EPR spectrum (*40*). The Fourier transform power spectra of aZ for periodicity analysis was calculated following published procedures (*41*).

For 49R1, we also determined the dissociation constant K_d of its Spβ complex by EPR, since its affinity with Spβ was too weak to be measured by ITC, as discussed below. Following published procedures for obtaining K_d values from EPR data (*21*), spectra of 49R1 titrated with various amounts of Spβ were obtained. $K_d = ([49R1] - [cx]_i)([Sp\beta]_i - [cx]_i)/[cx]_i$, where $[cx]_i$ was the equilibrium concentration of the complex in the mixture when the Spβ concentration was $[Sp\beta]_i$, and $h_i = h_{49R1}([49R1] - [cx]_i)/([49R1]) + h_{cx}([cx]_i/[49R1])$, where h_i was the non-normalized amplitude of the central line, after the ith addition of Spβ and h_{49R1} when no Spβ was added, with all spectra recorded under identical spectrometer settings (*21*). [49R1] was 68 μM in this experiment. h_{cx} was the amplitude of 49R1 when fully complexed with Spβ, a parameter to be determined with K_d. The curve fitting of the plot h_i versus $[Sp\beta]_i$ to determine K_d and h_{cx} was processed with the software Origin (OriginLab Corporation, Northampton, MA).

Accessibility experiments were done with a Varian E-109E spectrometer at 9.35 GHz, equipped with a loop-gap resonator (Molecular Specialties Inc., Milwaukee, WI) at room temperature (about 22 °C). Spin labeled protein samples (about 100 μM) in PBS7.4, with and without 5 mM nickel ethylenediamine-di(*o*-hydroxyphenyl acetic acid) (Ni-EDDA), were placed in gas permeable TPX sample tubes (Molecular Specialties Inc., Milwaukee, WI). Ni-EDDA was synthesized as described previously (*42*). Nitrogen gas was continuously purged around the sample tube during each measurement. The peak-to-peak amplitudes of the central line were monitored with microwave power of ~2 mW, and measurements as a function of microwave power began only after no further decrease in signal amplitude occurred, indicating complete removal of oxygen gas in samples. The amplitude values at a microwave power of 0.5 to 40 mW were analyzed following established methods (*42*) to give accessibility values (with 5 mM Ni-EDDA) for two protein samples with labeled residues in the junction region (R45R1 and K48R1).

RESULTS

Protein Characterization. The molecular masses of all proteins were within 2.5 Da of calculated values, with most less than 1 Da from their expected values, and the proteins were purified to contain no more than 10% impurity components, as indicated by SDS−PAGE. CD analysis of the spin labeled proteins showed helical contents of 76 ± 3%, similar to that of the native protein, or to those of other labeled spectrin proteins (*10, 16*). As mentioned in the Materials and Methods section, the helical content obtained from CD measurements is lower than the actual helical content. The finding that the replacement of a native residue by a spin labeled cysteine residue in this region did not affect helical content indicated that the replacements/mutations did not introduce large conformational changes.

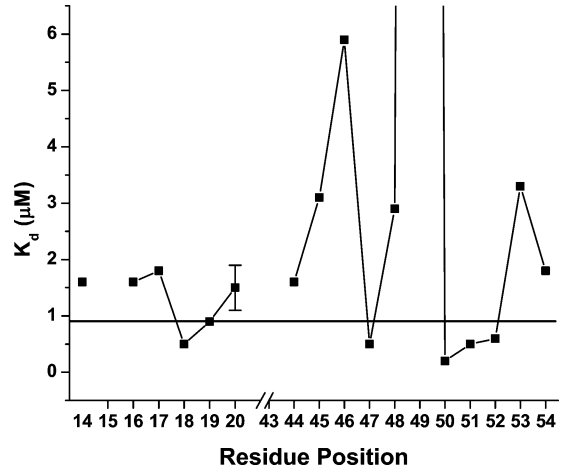

FIGURE 1: The dissociation constants, K_d, of spin labeled SpαΔ proteins with Spβ. With the exception of 49R1, the K_d was determined from ITC measurements, with 150−500 μM Spα titrated into 20−30 μM Spβ as described in the Materials and Methods section. A typical standard deviation (±0.4 μM) is shown for that of 20R1. The horizontal line was drawn at a K_d value of 0.9 μM for cysteine-less and Spα native protein. The value for 49R1 was obtained from EPR measurements (see Figure 2).

Association of Labeled Proteins with Spβ. The association equilibrium constants determined from ITC results were converted to dissociation constants. The average K_d value of Spα cysteine-less and native proteins was 0.9 ± 0.1 μM ($n = 3$), which agreed with the previously published value of a similar protein consisting of the first 156 residues of α-spectrin (*4, 11*). Most of the labeled SpαΔ proteins in this study exhibited K_d values ranging from 0.5 to 2 μM (Figure 1), similar to that of the native protein. For example, the K_d value for 20R1 was 1.5 ± 0.4 μM. However, the K_d values for 45R1, 46R1, 48R1, 49R1 and 53R1 were above 2 μM, with 45R1 at 2.9 μM, 46R1 at 5.9 μM, 48R1 at 3.1 μM and 53R1 at 3.3 μM. For 49R1, the heat released in the ITC experiments was not sufficient for K_d analysis. The K_d value from EPR measurements was 98 μM (Figure 2).

EPR Studies of Labeled Proteins in the Absence of Spβ. The structure of isolated Spα is known from NMR studies for the scanned regions (*8*), with the regions consisting of residues 14−20 being unstructured, residues 44−45 being in a helix without contact, residues 46−52 being unstructured, and residues 53−54 being in a helix bundled with other helices. Thus, the EPR studies of these regions in Spα alone provided validity and references for the EPR studies of them in the complex. The spectra of 14R1−20R1 were relatively simple (Figure 3), with rather narrow line-widths, indicating that the labeled cysteine side chains in these proteins exhibited relatively high mobility. Their ΔH^{-1} values were larger than 0.35 G^{-1} (Figure 4), with the largest value (0.60

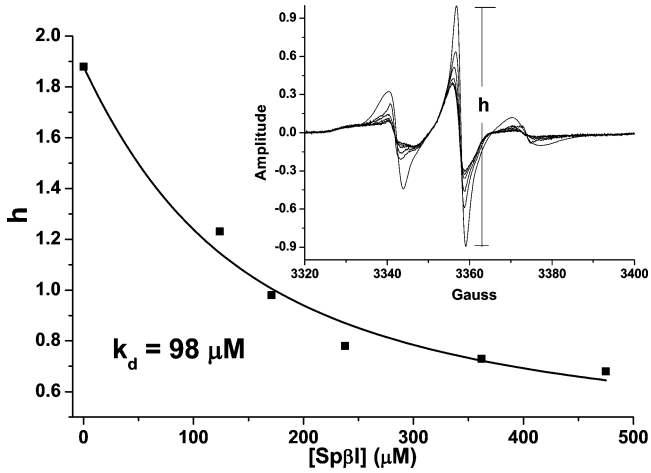

FIGURE 2: The peak-to-peak amplitudes of the central line (*h*) of 49R1 vary in the presence of various amounts of Spβ. The concentration of 49R1 in all samples was 68 μM. The data points were fitted, as described in the Materials and Methods section, to give the curve in the plot and a K_d value of 98 μM. The R^2 value for the fit was 0.979. The inset panel shows the EPR spectra of 49R1 with various amounts of Spβ.

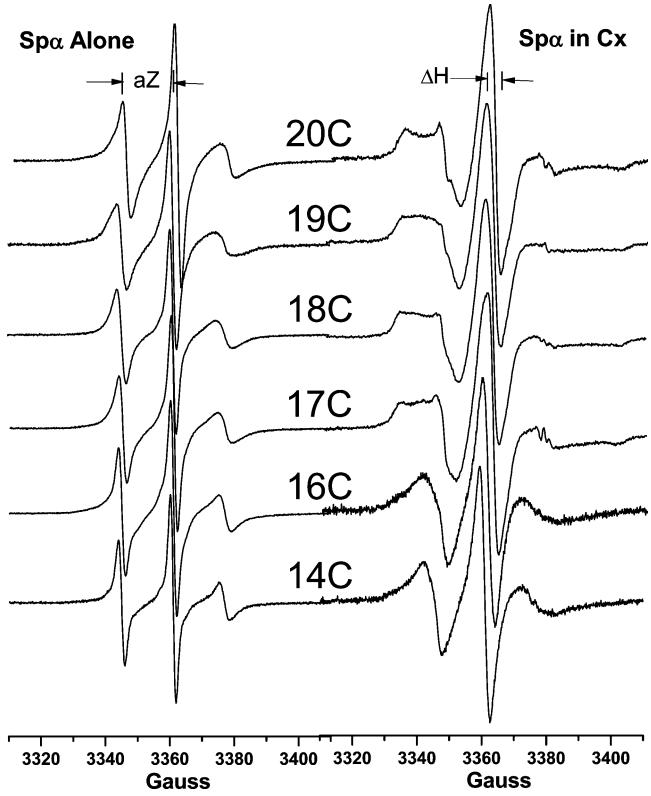

FIGURE 3: EPR spectra of labeled Sp$\alpha\Delta$ 14R1−20R1 alone (left) and in the presence of a 2 molar excess of Spβ (right). Raw spectra of labeled proteins at 60 μM in PBS buffer containing 40% glycerol were acquired at 20 °C. Signals from nonspecific labeling were removed from the raw spectra. The spectra of Spα alone generally consisted of about 15% nonspecific background labeling. Some of the spectra of Spα in complex also consisted of the signal of labeled glutathione (see Materials and Methods section) and the signal of the uncomplexed (Spα alone) component. These signals were subtracted also. No labeled 15C sample was prepared due to the lack of protein expression of this single cysteine protein. The parameters *aZ* and ΔH are also indicated.

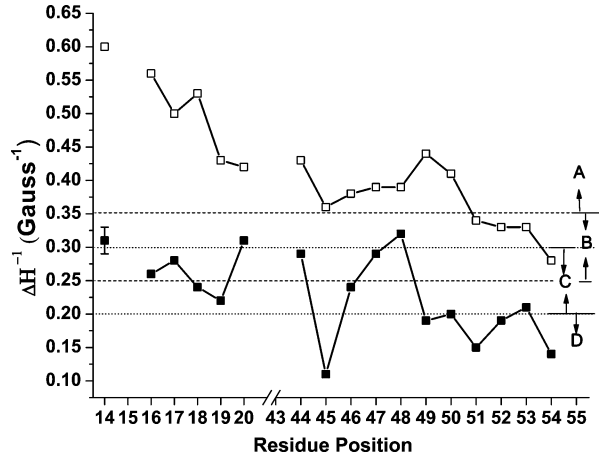

FIGURE 4: Inverse central line width (ΔH^{-1}) values varied as a function of the labeled position of Spα alone (open squares) and in the complex (filled squares). The values of Spα in the complex are all lower than the corresponding ones of Spα alone. The plot is divided, by horizontal lines, into four regions (A, B, C and D, as marked on the right-hand side of the plot), based on published values of ΔH^{-1} of residues at different locations in T4 lysozyme (*40*). Values above 0.35 G^{-1} (A) are for those in the unstructured region, values between 0.35 and 0.25 G^{-1} (B) are for those of exposed residues in a helix, values between 0.30 and 0.20 G^{-1} (C) are for those in a helix but with tertiary contact, and values below 0.2 G^{-1} (D) are for those buried in a helix. The values for Spα alone suggest that the residues from 14 to 20 and those from 44 to 50 are in an unstructured conformation. However, in the complex, these residues are now in either a tertiary contact or a buried region. A periodicity of about 3.5 is also observed for those between 45 and 51, with residues at 45, 49 and 51 having smaller ΔH^{-1} values.

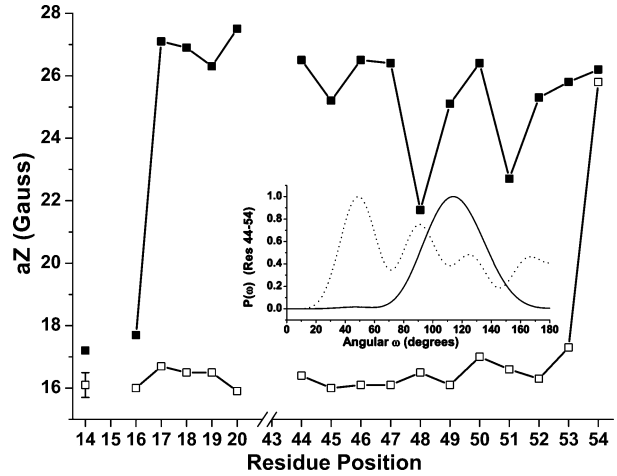

FIGURE 5: The values of spectral widths between the low field peak and the central peak (*aZ*, see Figure 3, a value related to the hyperfine separation value) were plotted against the position of the label in Spα when Spα was either alone (open squares) or in complex (filled squares). The values remain at about 16−17 G for Spα alone, except for 54R1. However, in the complex, only 14R1 and 16R1 remained around 17−18 G. Substantial increases, to 26−28 G, were observed for 17R1−20R1. For 44R1 to 54R1, the values ranged between 22 and 27 G, with an apparent periodicity of 3.5 for residues 46−52. The Fourier transform power spectrum for residues 44−54 in the complex (inset, solid line) showed an angular frequency of about 110, which was generally considered to indicate a helical conformation. The dotted line was that in Sp$\alpha\Delta$R1 alone.

G^{-1}) at 14R1 and the smallest value (0.42 G^{-1}) at 20R1. The *a*Z values were about 16−17 G (Figure 5). The spectra of 44R1−54R1 alone (Figure 6), except for 54R1, were still relatively simple. A small amount of a more immobilized component, marked by an arrow in Figure 6, was also observed in the spectra of 45R1−47R1 and of 51R1−53R1.

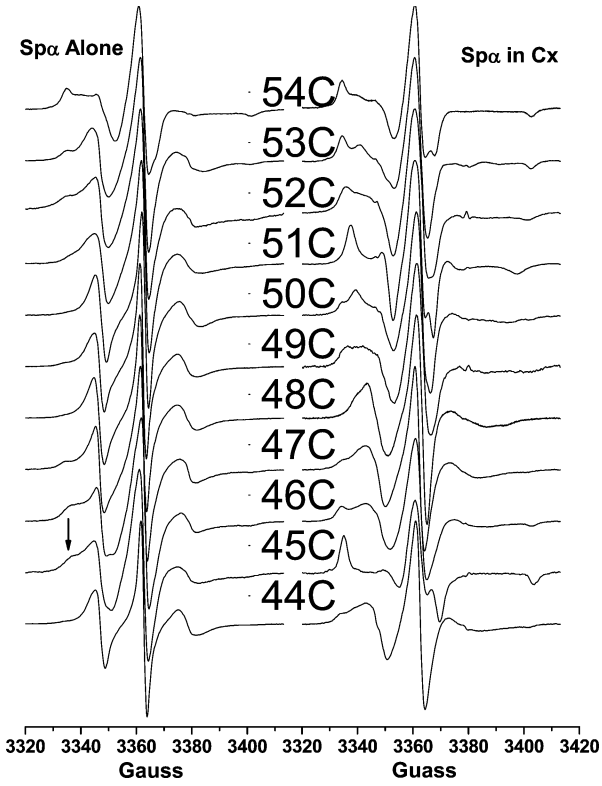

FIGURE 6: EPR spectra of labeled 44R1−54R1 of Spα alone (left) and in the presence of a 2 molar excess, except for 49R1 of 5 molar excess, of Spβ (right). Sample conditions and nonspecific signal removal are the same as those described for Figure 3. Spectra for Spα alone were relatively simple with narrow line widths, except for that of 54R1. A small amount of a more immobilized component, marked by an arrow, were also observed in the spectra of 45R1−47R1 and of 51R1−53R1. The spectra of Spα in the complex differ substantially from those of Spα alone.

The signals were generally slightly broader, and thus ΔH^{-1} values were smaller than those of 14R1−20R1, ranging from 0.3 to 0.4 G^{-1} (Figure 4). The *aZ* values, except again that of 54R1, were similar to those of 14R1−20R1, about 16−17 G (Figure 5). The EPR data agreed well with the NMR solution structure. Residues 53 and 54 are in Helix A_1 of the triple helical bundle structural domain, with residue 53 more exposed to the solvent and thus more similar to residues 44 and 45 and different from the more buried residue 54.

The Ni-EDDA (5 mM) accessibility values for residues 45 and 48 were both 0.28. Values larger than 0.25 are considered to be from exposed residues, whereas those smaller than 0.25 are considered to be from buried residues (*45*).

The values of ΔH^{-1} and $\langle H^2 \rangle^{-1}$ of a spin labeled residue have been used to indicate whether the residue is in a loop/surface, loop/contact, helix/surface, helix/contact or helix/buried region (*43*). Figure 7 shows that using these values to assign each residue to a structure for all labeled residues in isolated Spα sample agreed remarkably well with the NMR structure.

EPR Studies of Labeled Proteins in the Presence of Spβ. The spectra of all labeled SpαΔ proteins in the presence of Spβ differed from those in the absence of Spβ (Figures 3 and 6). The spectra were generally broader and more complex. For the 14R1−20R1 group, the spectra of 14R1 and 16R1 were rather similar to each other, but were quite different from those of 17R1−20R1 (Figure 3). All ΔH^{-1} values decreased to below 0.35 G^{-1}, with the lowest at 19R1 (0.22 G^{-1}) and the highest at 20R1 (0.31 G^{-1}) (Figure 4). The *aZ* values of 14R1 and 16R1 (about 17−18 G) were only slightly higher than the corresponding ones without Spβ (Figure 5). However, the values increased to around 26−27 G for 17R1−20R1 upon binding Spβ.

For the 44R1−54R1 group, the spectra of 45R1, 51R1 and 54R1 were similar to those of highly immobilized spectra. Their ΔH^{-1} values (well below 0.20 G^{-1}) also suggested that the motions of the labels at these positions were most restricted (Figure 4). The ΔH^{-1} values of this group varied from 0.32 G^{-1} (for 48R1) to 0.11 G^{-1} (for 45R1), suggesting that these residues in the complex were either in tertiary contacts or in a buried region.

The Ni-EDDA (5 mM) accessibility value for residue 45 was 0.15 and for residue 48 was 0.42, indicating residue 45 in the complex was buried presumably in the core of the triple helical bundle, whereas residue 48 was exposed to solvent (*45*).

The values of ΔH^{-1} and $\langle H^2 \rangle^{-1}$ of residues in the complex suggested that all residues were now in regions with a helical conformation (Figure 7). This is in agreement with our earlier CD studies indicating that an increase in the total helical content occurs upon complex formation (*3*).

An examination of the periodic dependence of ΔH^{-1} or *aZ* parameters on residue position (Figure 4 or 5) showed that the 3.5 periodicity for a helix was not obvious, especially for ΔH^{-1} values. Some published works involving ΔH^{-1} values as a function of residue position show very regular periodicity of about 3.5 for helices (*40*), while others show less regular periodicity (*28*). The periodic dependence on residue position was more obvious for the *aZ* parameter for the region of residues 44−54 (Figure 5). The Fourier transform power spectrum for residues 44−54 in the complex showed an angular frequence of about 110, indicating a helical conformation (*44*).

DISCUSSION

The N-terminal partial domain (Helix C′, spanning residues 21−45) of erythroid α-spectrin has been predicted (*7*) and shown experimentally (*3, 22*) to be the component of α-spectrin interacting with the β-spectrin C-terminal region. Many mutations in Helix C′ have been shown to be clinically significant mutations leading to hereditary elliptocytosis or pyropoikilocytosis (*23, 24*). Helix C′ is flanked by two unstructured segments, one of 20 residues upstream of Helix C′ (residues 1−20) and another 7 residues downstream of Helix C′ (residues 46−52, the junction region) (*8*). Since these two segments are unstructured and are not part of Helix C′, they would not be expected to be involved in helical bundling with the partial domain helices in β-spectrin upon complex formation. However, our recent solution NMR studies suggest that some parts of these two unstructured segments undergo conformational changes upon binding β-spectrin to form tetramers (*11*). Unfortunately no structural information was obtained due to NMR line broadening in the highly asymmetric complex (*11*). In the current study, we used cysteine-scanning, ITC and spin label EPR methods to determine the importance of several of these residues and the conformation of these two segments in the αβ complex.

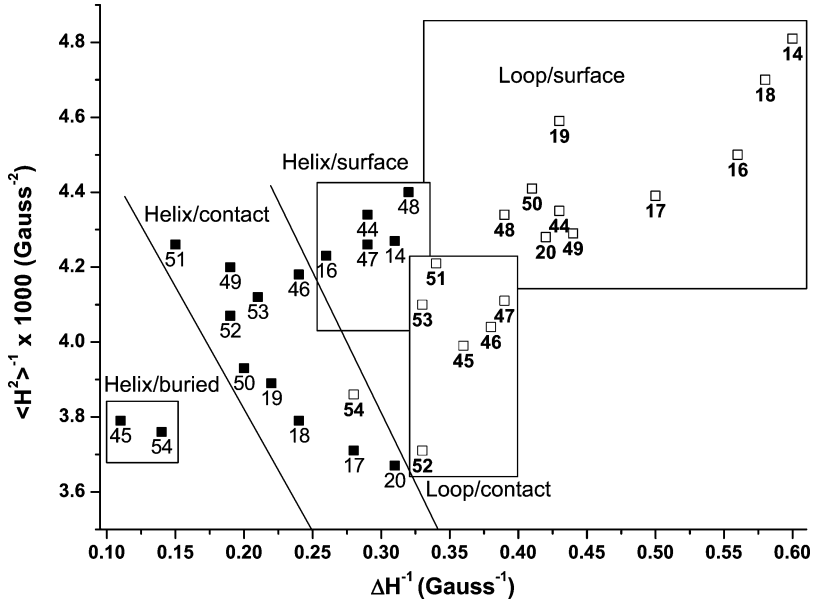

FIGURE 7: Reciprocal plot of $\langle H^2 \rangle$ of the EPR spectrum versus ΔH^{-1} of all samples, SpαΔR1 alone (open squares) and in complex (filled squares). The numbers are the positions of the labeled residues. The values in Figure 2b of ref *43* are used to assign the structural elements to the residues. The NMR structure of Spα alone shows residues 14−20 and residues 46−52 unstructured, whereas residues 44, 45 and 53 on helix surface and residue 54 buried in the triple helical bundle. Thus, the EPR data of SpαΔR1 alone agree remarkably well with the NMR structure. According to the structural assignments, no residues in the complex are in loops (unstructured), with residues 14, 16, 44, 47, 48 on the surface of a helix, residues 17−20, 46, 49−53 on a helix with contacts, and residues 45 and 54 on a helix but buried.

The affinity in the association with β-spectrin model protein when each of the Spα residues, scanning positions 14−20, was replaced with a spin labeled cysteine residue remained similar to that for WT. The K_d values were slightly higher for G14R1, K16R1, V17R1 and T20R1, about 1.5−2 μM, than for WT, which is about 1 μM at 25 °C.

For the region scanning residues 44−54, the replacement of residues 45, 46, 48 or 49 with a spin labeled cysteine residue reduced the affinity for association with a β-spectrin model protein, with K_d values 3 times higher for R45R1 and K48R1, and 6 times higher for G46R1 than for WT. The most severe one was L49R1, where ITC methods were only able to estimate that its K_d value was larger than 30 μM. However, by using EPR methods, we obtained a K_d value of about 100 μM at 25 °C. A recently published publication (*12*) reported their ITC results at 23 °C for a similar system, but with different residue replacements, with K_d values >200 μM for R45S, 14 μM for R45T, 3.7 μM for G46V, 0.5 μM for K48R, 30 μM for L49F and 0.4 μM for WT. Since our studies used a residue with the same side chain (spin labeled side chain of cysteine) for the replacement at each of these positions, we are able to directly compare them with each other, and the values showed the following order: L49 > G46 > K48. Residue 45 is in Helix C′, which is involved in helical bundling upon complex formation, and yet the effect of replacing R with spin labeled cysteine residue at position 45 resulted in K_d similar to K48 replacement, the last one in the above order. Thus, the residues following Helix C′ were clearly very important in $\alpha\beta$ interactions to form tetramers.

Our EPR results showed that, in the presence of Spβ, the motional characteristics of residues 14−16, upstream of Helix C′, were similar to those observed by others for residues in unstructured regions (*25, 26*), and therefore these residues remained in an unstructured conformation and were probably not important in interactions during tetramer formation. However, residues 17−20, though in an unstructured conformation in the absence of Spβ, now exhibited EPR properties similar to those of helical residues in the presence of Spβ. The ΔH^{-1} values agreed well with other spin labeling EPR studies of helices in either "noninteracting helical surface region" (*27, 28*) or in tertiary contacts (*29*). These values also agreed well with the values from our earlier spin label EPR studies of residues 21−30 (the first ten residues in Helix C′) in the absence of β-spectrin, ranging between 0.25 and 0.40 and following a periodicity of 3.5 residues (*10*). It is interesting to note that in coiled coil prediction, for example with the Marcoil program (*30*), the probabilities for residues 17−20 in the first-156-residue fragment to form a helical coil are very high (V17, 42%; L18, 55%; E19, 71% and T20, 77%). Thus, we believe that residues 17−20 are involved in tetramer formation and appear likely to become helical upon binding β-spectrin. This conclusion is in good agreement with our previous finding that α-spectrin lacking the first 22 residues exhibits slightly lower affinities than WT (*31*). This is also in good agreement with our CD findings that, upon complex formation, a 10% increase in total helical content was observed (*3*).

A working 3D model of Helices A′, B′ and C′ bundling (Figure 8), based on sequence alignment (*3*) and guided by the NMR structure of the first complete triple helical bundle for relative positions of the three helices (*8*), suggests that residues 17−20 in α-spectrin are close to the "bottom" of the last structural domain as well as the end of Helix B′ of β-spectrin (which ends at residue 2070) (*10*), and to the region following Helix B′, which has been assumed to be unstructured (Figure 8). Little structural information on β-spectrin is currently available. In particular, the negatively charged side chain of E19 of α-spectrin may interact with K1997, R2001, R2004, R2006, K2070, K2077 or R2079 of β-spectrin to stabilize the helical bundle.

Similarly, residues downstream of Helix C′ at positions 46−52 were also no longer in an unstructured conformation

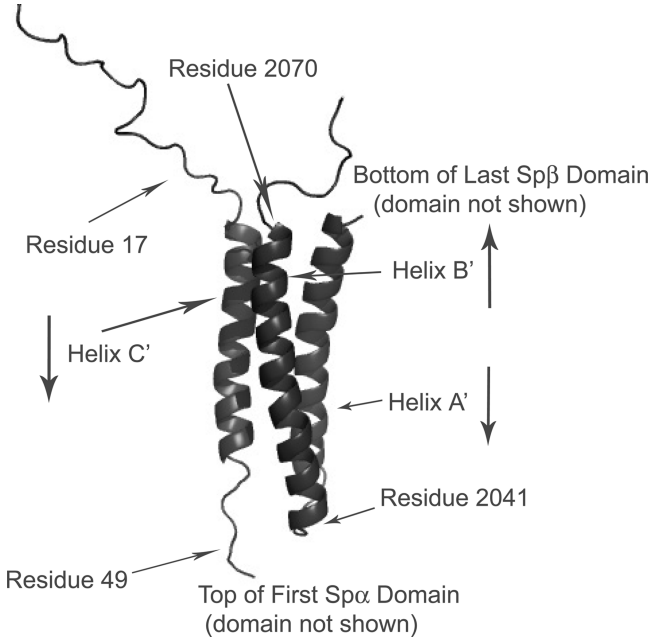

FIGURE 8: A working 3D model of Helices A′, B′ and C′ bundling, based on sequence alignment (*3*) and guided by the NMR structure of the first complete triple helical bundle structure domain (*8*) for relative positions of the three helices. We suggest that a segment of the unstructured region upstream of Helix C′ and the junction region (residues 46−52) of Spα becomes helical upon binding Sp*β*.

in the presence of *β*-spectrin. Their EPR parameter values were also similar to those of helical residues either exposed or with tertiary contacts. In addition, values of *aZ* exhibited a periodicity of 3.5 residues in this region. The probabilities for these residues to form a coil conformation were very high (above 70% for G46, Q47, K48, L49 and E50; about 54% for D51 and 21% for S52). Potentially, K48 may interact with D2042 or E2045 at the start of Helix B′. In addition, L49 with V2041 (of the loop between Helix A′ and Helix B′ in our working model), V2044 (in Helix B′), L2047 (in Helix B′) and I2048 (in Helix B′) form a hydrophobic cluster that favors helical bundling. The charged residues (K48, E50 and D51) may also interact with residues on the "top" of the first structural domain.

In an earlier study, we detected an increase in helicity in the two model proteins upon binding (*3*). Based on high resolution NMR results, we first suggest that the regions flanking Helix C′ undergo conformational changes, from unstructured to helical, upon binding *β*-spectrin (*10*). Now we experimentally detected such changes. The current study pinpoints the region responsible for such helical content increase in the complex. It is possible that *β*-spectrin undergoes similar changes (*11*).

Our studies indicate that the junction region following Helix C′ is also involved in the interaction interface with *β*-spectrin. However, our data do not agree with a recent suggestion that residue 48 is not in the tetramer interface (*12*).

Our earlier NMR studies of the clinical R45T and R45S mutations show that the reduction in affinity at this position is due to perturbation of the interactions upon association (*32*) and is not due to large conformational changes of Spα, as suggested earlier (*9*). We suggest that a single mutation at positions 46, 48 or 49, which did not affect their helical contents and thus did not induce large conformational changes, may perturb interactions with specific residues in *β*-spectrin. This suggestion may explain why K48R replacement, which results still a positively charged side chain at position 48, does not exhibit an affinity different from that of WT (*12*), but our K48R1 exhibited a 3-fold decrease in dissociation constant value.

Two mechanisms have been suggested to rationalize conformational changes upon ligand binding (*33, 34*): induced-fit (*35*) and preexisting equilibrium dynamics (*36*). With preexisting equilibrium dynamics, it is possible that the region spanning residues 17−52 in α-spectrin exhibits conformational heterogeneity. Flexibility within regions of the protein allows it to adopt new conformation and, in turn, to effectively associate with its binding partner.

The genetics of hereditary pyropoikilocytosis suggest that patients typically fall into one of three categories: (i) they may be homozygous for a structural variant of spectrin, typically located in the region of spectrin α*β*-heterodimer self-association, (ii) they may be compound heterozygotes for structural variants of the self-association site, or (iii) they may be heterozygous for a single structural variant of spectrin self-association and possess a second, unknown defect that contributes to spectrin deficiency (*37*). Our studies suggest that residues 17−52, not just residues 21−45 that form the partial domain in α-spectrin, are important in determining the association affinity with *β*-spectrin. Mutations that affect the propensity for helical formation, hydrophobic clustering and/or salt-bridge stabilization of the bundled helices would affect spectrin tetramer formation and may lead to blood disorders. For example, for L49F mutation, in comparing Phe with Leu, the helical propensity (*38*) decreases, making the mutant less favorable for helix formation, and the hydrophathy index (*39*) also decreases, destabilizing the hydrophobic cluster discussed above. Similar mechanisms can be applied to L49H and L49R1. Thus, the affinity of these mutants with *β*-spectrin decreases and the concentration of spectrin tetramers decreases accordingly. For the K48R mutation, the salt-bridge remains and thus exhibits little effect on association affinity, whereas for K48R1, the salt-bridge interaction is no longer possible as a mechanism to lower association affinity.

REFERENCES

1. Ungewickell, E., and Gratzer, W. (1978) Self association of human spectrin: A thermodynamic and kinetic study. *Eur. J. Biochem. 88*, 379–385.
2. DeSilva, T. M, Peng, K. C, Speicher, K. D., and Speicher, D. W. (1992) Analysis of human red cell spectrin tetramer (head-to-head) assembly using complementary univalent peptides. *Biochemistry 31*, 10872–10878.
3. Mehboob, S., Luo, B. H., Patel, B. M., and Fung, L. W.-M. (2001) α*β* spectrin coiled coil association at the tetramerization site. *Biochemistry 40*, 12457–12464.
4. Mehboob, S., Jacob, J., May, M., Kotula, L., Thiyagarajan, P., Johnson, M. E., and Fung, L. W.-M. (2003) Structural analysis of the alpha N-terminal region of erythroid and nonerythroid spectrins by small-angle X-ray scattering. *Biochemistry 43*, 14702–14710.
5. Menhart, N., Mitchell, T., Lusitani, D., Topouzian, N., and Fung, L. W.-M. (1996) Peptides with more than 106-amino acid motif are needed to mimic the structural stability of spectrin. *J. Biol. Chem. 271*, 30410–30416.
6. Morrow, J. S., Speicher, D. W., Knowles, W. J., Hsu, C. J., and Marchesi, V. T. (1980) Identification of functional domains of human erythrocyte spectrin. *Proc. Natl. Acad. Sci. U.S.A. 77*, 6592–6596.

7. Tse, W. T., Lecomte, M. C., Costa, F. F., Garbarz, M., Feo, C., Boivin, P., Dhermy, D., and Forget, B. G. (1990) Point mutations in the beta-spectrin gene associated with alpha I/74 hereditary elliptocytosis. Implications for the mechanism of spectrin dimmer self-association. *J. Clin. Invest. 86*, 909–916.
8. Park, S., Caffrey, M. S., Johnson, M. E., and Fung, L. W.-M. (2003) Solution structural studies on human erythrocyte α-spectrin tetramerization site. *J. Biol. Chem. 278*, 21837–21844.
9. Grum, V. L., Li, D., MacDonald, R. I., and Mondragon, A. (1999) Structures of two repeats of spectrin suggest models of flexibility. *Cell 98*, 523–535.
10. Mehboob, S., Luo, B. H., Fu, W., Johnson, M. E., and Fung, L. W.-M. (2005) Conformational studies of the tetramerization site of human erythroid spectrin by cysteine-scanning spin labeling EPR methods. *Biochemistry 42*, 14702–14710.
11. Long, F., McElheny, D., Jiang, S., Park, S., Caffrey, M. S., and Fung, L. W.-M. (2007) Conformational change of erythroid a-spectrin at the tetramerization site upon binding β-spectrin. *Protein Sci. 16*, 2519–2530.
12. Gaetani, M., Mootien, S., Harper, S., Gallagher, P. G., and Speicher, D. W. (2008) Structural and functional effects of hereditary hemolytic anemia-associated point mutations in the alpha spectrin tetramer site. *Blood 111*, 5712–5720.
13. Morle, L., Roux, A. F., Alloisio, N., Pothier, B., Starck, J., Denoroy, L., Morle, F., Rudigoz, R.-C., Forget, B. G., Delaunay, J., and Godet, J. (1990) Two elliptocytogenic alpha I/74 variants of the spectrin alpha I domain. *J. Clin. Invest. 86*, 1088–1100.
14. Marchesi, S. L., Knowles, W. J., Morrow, J. S., Bologna, M., and Marchesi, V. T. (1986) Abnormal spectrin in hereditary elliptocytosis. *Blood 67*, 141–151.
15. Ranganathan, S., Menhart, N., Topouzian, N., and Fung, L. W.-M. (2001) Laboratory method to study mutational effects on human erythrocyte spectrin tetramerization. *Am. J. Hematol. 67*, 247–251.
16. Cherry, L., Fung, L. W.-M., and Menhart, N. (2000) Flexibility of the alpha-spectrin N-terminus by EPR and fluorescence polarization. *Biophys. J. 79*, 526–535.
17. Lusitani, D. M., Qtaishat, N., LaBrake, C. C, Yu, R. N., Davis, J., Kelley, M. R., and Fung, L. W.-M. (1994) The first human α-spectrin structural domain begins with a serine. *J. Biol. Chem. 269*, 25955–25958.
18. Luo, B. H., Mehboob, S., Hurtuk, M. G., Pipalia, N. H., and Fung, L. W.-M. (2002) Important region in the beta spectrin C-terminus for spectrin tetramer formation. *Eur. J. Haematol. 68*, 73–79.
19. Greenfield, N., and Fasman, G. D. (1969) Computer circular dichroism spectra for the evaluation of protein conformation. *Biochemistry 8*, 4108–4116.
20. Antoniou, C., and Fung, L. W.-M. (2008) Potential artifacts in using a glutathione-S-transferase fusion protein system and spin labeling electron paramagnetic resonance methods to study protein-protein interactions. *Anal. Biochem. 376*, 160–162.
21. Liao, H., Ellena, J., Lu, L., Szabo, D., Cafiso, D., and Castle, D. (2007) Secretory carrier membrane protein SCAMP2 and phosphatidylinositol 4,5-bisphosphate interactions in the regulation of dense core vesicle exocytosis. *Biochemistry 46*, 10909–10920.
22. Nicolas, G., Pedroni, S., Fournier, C., Gautero, H., Craescu, C., Dhermy, D., and Lecomte, M. C. (1998) Spectrin self-association site: characterization and study of beta-spectrin mutations associated with hereditary elliptocytosis. *Biochem. J. 332*, 81–89.
23. Delaunay, J. (2007) The molecular basis of hereditary red cell membrane disorders. *Blood Rev. 21*, 1–20.
24. Delaunay, J., and Dhermy, D. (1993) Mutations involving the spectrin contact site: clinical expression and alterations in specific function. *Semin. Hematol. 30*, 21–33.
25. Zhang, F., Chen, Y., Kweon, D. H., Kim, C. S., and Shin, Y. K. (2002) The four-helix bundle of the neuronal target membrane SNARE complex is neither disordered in the middle nor uncoiled at the C-terminal region. *J. Biol. Chem. 277*, 24294–24298.
26. Columbus, L., and Hubbell, W. L. (2004) Mapping backbone dynamics in solution with site-directed spin labeling: GCN-58 bZip Free and Bound to DNA. *Biochemistry 43*, 7273–7287.
27. Columbus, L., Kalai, T., Jeko, J., Hideg, K., and Hubbell, W. L. (2001) Molecular motion of spin labeled side chains in a-helices: Analysis by variation of side chain structure. *Biochemistry 40*, 3828–3846.
28. Isas, J. M., Langen, R., Haigler, H. T., and Hubbell, W. L. (2002) Structure and dynamics of a helical hairpin and loop region in annexin 12: A site-directed spin labeling study. *Biochemistry 41*, 1464–1473.
29. Guo, Z., Cascio, D., Hideg, K., and Hubbell, W. L.,. (2008) Structural determinants of nitroxide motion in spin-labeled proteins. Solvent exposed sites in helix B of T4 lysozyme. *Protein Sci. 17*, 228–239.
30. Delorenzi, M., and Speed, T. (2002) An HMM model for coiled-coil domains and a comparison with PSSM-based predictions. *Bioinformatics 18*, 617–625. The web program address is http://www.isrec.isb-sib.ch/webmarcoil/webmarcoilC1.html.
31. Lusitani, D., Menhart, N., Keiderling, T. A., and Fung, L. W.-M. (1998) Ionic strength effect on the thermal unfolding of α-spectrin peptides. *Biochemistry 37*, 16546–16554.
32. Park, S., M. S., Johnson, M. E., and Fung, L. W.-M. (2002) Nuclear magnetic resonance studies of mutations at the tetramerization region of human alpha spectrin. *Blood 100*, 283–288.
33. Xu, Y., Colletier, J. Ph., Jiang, H., Silman, I., Sussman, J. L., and Weik, M. (2008) Induced-fit or pre-existing dynamics? Lessons from protein crystallography and MD simulations on acetylcholinesterase and implications for structure-based drug design. *Protein Sci. 17*, 601–605.
34. Goh, C. S., Milburn, D., and Gerstein, M. (2004) Conformational changes associated with protein-protein interactions. *Curr. Opin. Struct. Biol. 14*, 104–109.
35. Koshland, D. E. (1958) Application of a theory of enzyme specificity to protein synthesis. *Proc. Natl. Acad. Sci. U.S.A. 44*, 98–104.
36. Monod, J., Wyman, J., and Changeux, J. P. (1965) On the nature of allosteric transitions: A plausible model. *J. Mol. Biol. 12*, 88–118.
37. Coetzer, T., Palek, J., Lawler, J., Liu, S. C., Jarolim, P., Lahav, M., Prchal, J. T., Wang, W., Alter, B. P., Schewitz, G., Mankad, V., Galianello, R., and Cao, A. (1990) Structural and functional heterogeneity of alpha spectrin mutations involving the spectrin heterodimer self-association site: relationships to hematologic expression of homozygous hereditary elliptocytosis and hereditary pyropoikilocytosis. *Blood 75*, 2235–2244.
38. Pace, C. N., and Scholtz, J. M. (1998) A helix propensity scale based on experimental studies of peptides and proteins. *Biophys. J. 75*, 422–427.
39. Kyte, J., and Doolittle, R. F. (1982) A simple method for displaying the hydropathic character of a protein. *J. Mol. Biol. 157*, 105–132.
40. Mchaourab, H. S., Lietzow, M. A., Hideg, K., and Hubbell, W. L. (1996) Motion of spin-labeled side chains in T4 lysozyme. Correlation with protein structure and dynamics. *Biochemistry 35*, 7692–7704.
41. Perozo, E., Cortes, D. M., and Cuello, L. G. (1998) Three-dimensional architecture and gating mechanism of a K+ channel studied by EPR spectroscopy. *Nat. Struct. Biol. 5*, 459–469.
42. Altenbach, C., Greenhalgh, D. A., Khorana, H. G., and Hubbell, W. L. (1994) A collision gradient method to determine the immersion depth of nitroxides in lipid bilayers: application to spin-labeled mutants of bacteriorhodopsin. *Proc. Natl. Acad. Sci. U.S.A. 91*, 1667–1671.
43. Fanucci, G. E., and Cafiso, D. S. (2006) Recent advances and applications of site-directed spin labeling. *Curr. Opin. Struct. Biol. 16*, 644–653.
44. Brown, L. J., Sale, K. L., Hills, R., Rouviere, C., Song, L., Zhang, X., and Fajer, P. G. (2002) Structure of the inhibitory region of troponin by site directed spin labeling electron paramagnetic resonance. *Proc. Natl. Acad. Sci. U.S.A. 99*, 12765–12770.
45. Oh, K. J., Barbuto, S., Meyer, N., Kim, R. S., Collier, R. J., and Korsmeyer, S. J. (2005) Conformational changes in BID, a pro-apoptotic BCL-2 family member, upon membrane binding. *J. Biol. Chem. 280*, 753–767.

BI800840P